EFFECTS OF RADIATIVE TRANSFER ON HELIOSEISMIC SIGNATURES IN ACTIVE REGIONS

Charles Lindsey
NorthWest Research Associates
and
Juan Fontenla
Laboratory for Astrophysics and Space Physics
University of Colorado

Background

Efforts to model sunspots based on helioseismic signatures

Moradi et al. (2010): A general review.

Cameron, Gizon, Schunker & Pieterila (2011) represent helioseismic signatures in terms of a classical scattering problem, illuminating an active region by plane waves from a distant source and examining the scattered component.

Braun, Birch, Crouch & Rempel (2011) examine issues related to effects of filtering used with time-distance seismology, including holography, and resolving major puzzles in intuitive terms.

Lindsey, Cally & Rempel (2010) use ingression control correlations as a means of discriminating thermal from magnetic anomalies in sunspot umbrae.

Aspects in Seismic Discrimination

- Whole-model diagnostics: The scattered wave of Cameron et al. (2011) is influenced by the entirety of the anomaly, as far as we know. This leaves the problem of both spatial and magnetic vs thermal discrimination open. However, it is insensitive to effects of non-adiabatic acoustics on local helioseismic signatures.

- Discrimination of model components: Ingression control-correlation statistics offer this, but probably require an account of non-adiabatic acoustics in the outer atmospheres of both active regions and the quiet Sun.

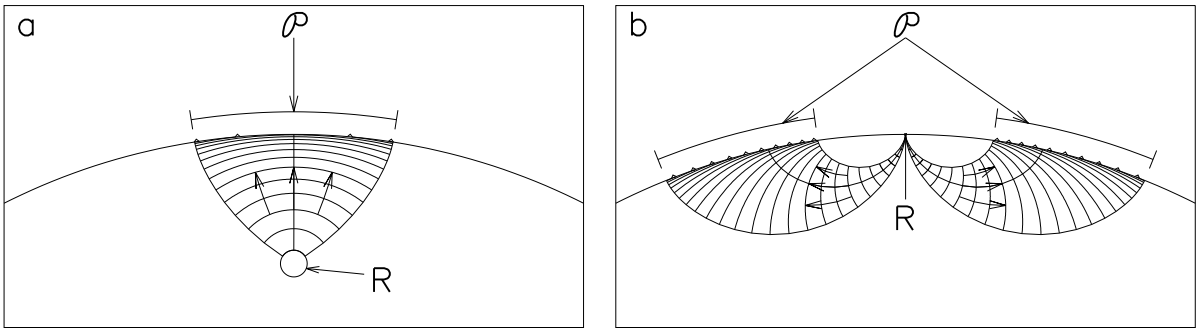

Figure 1: Diagrams representing waves configurations for superjacent-vantage holography (panel a) and subjacent-vantage holography (panel b). Superjacent-vantage holography (a) is focused on a submerged source, R, from an overlying pupil, $\mathcal{P}$. Subjacent-vantage holography (b) is focused on a surface source from a displaced, or surrounding pupil.

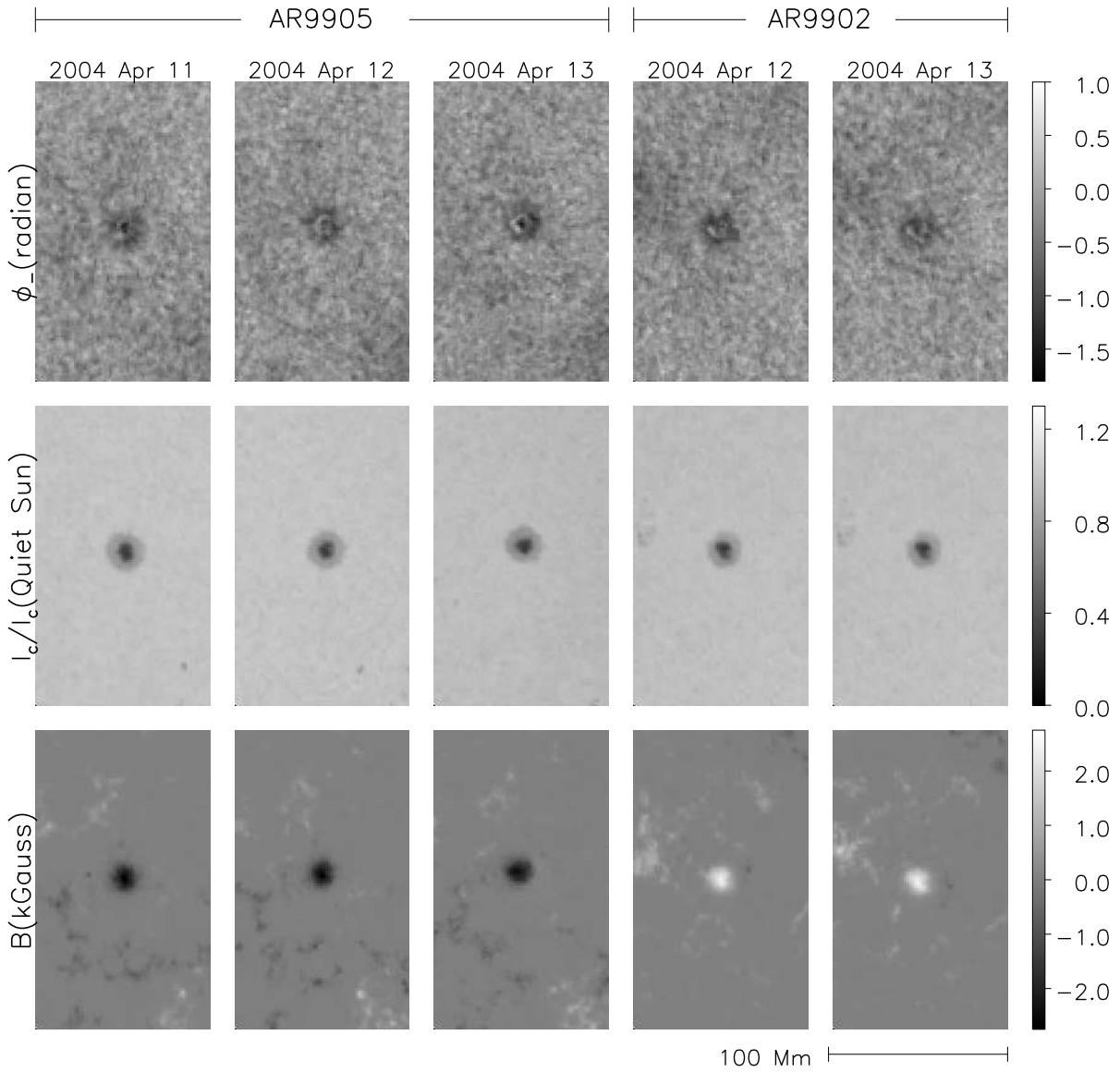

Figure 2: Maps of the phase, ϕ_-, of the local ingression control correlation, C_{LC-}, for two nearly circular sunspots. Top row shows ϕ_- in the 3.5–4.5 mHz spectrum computed over an annular pupil whose radial range is 16.5–48.0 Mm. Middle row shows concurrent, cospatial MDI continuum-intensity maps. Bottom row shows concurrent, cospatial line-of-sight MDI magnetograms.

Spectral Dependence
of Ingression Control Correlation Signatures

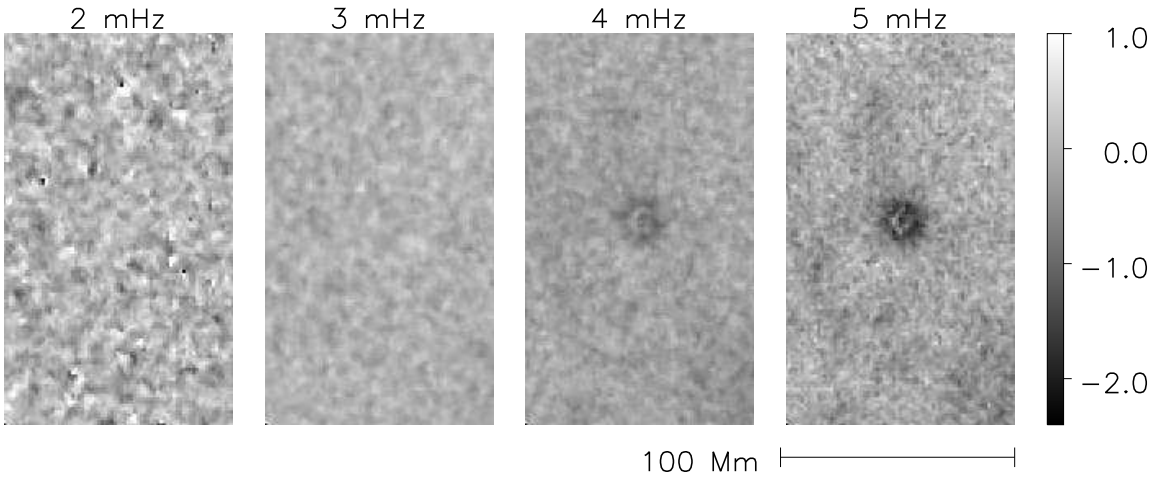

Figure 3: Phase, ϕ_-, of the ingression control correlation, C_{LC-}, integrated over 1-mHz passbands centered at—proceeding from left-to-right—2, 3, 4, and 5 mHz is mapped in the neighborhood of AR9902 on 2004 April 12. The gray scale (right) calibrates the phase of the control correlation in radians. The penumbral and center-umbral phase signatures increase sharply with frequency, ν, from insignificance at 2 mHz to clearly significant at 4 and 5 mHz.

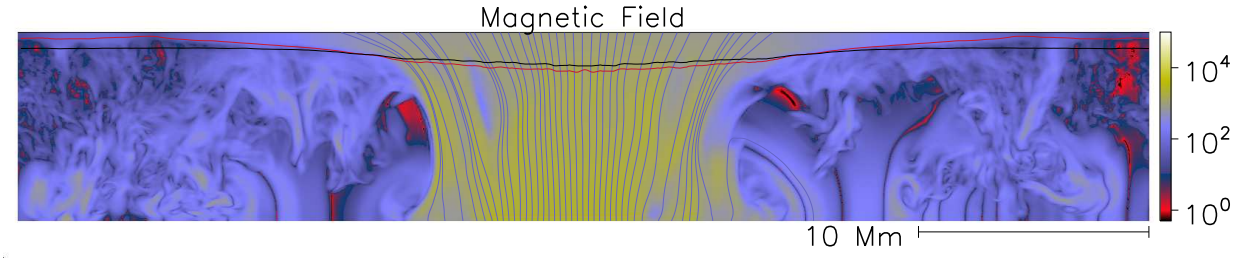

Figure 4: Vertical cut through a 3-D map of the absolute value, $|\mathbf{B}|$, of magnetic induction in the LRRMC-25 simulation, averaged over the period 25 $\pm$ 1 hr. The color bar (right) calibrates $|\mathbf{B}|$ in Gauss. The light-blue curves represent magnetic streamlines projected into the plane of the cut. The heavy blue curve just beneath the top boundary marks the photosphere of the medium averaged over azimuth. The red curve marks the surface on which β is unity, similarly averaged over azimuth.

Vertically propagating waves in a vertical magnetic field are insensitive to the "magnetic anomaly."

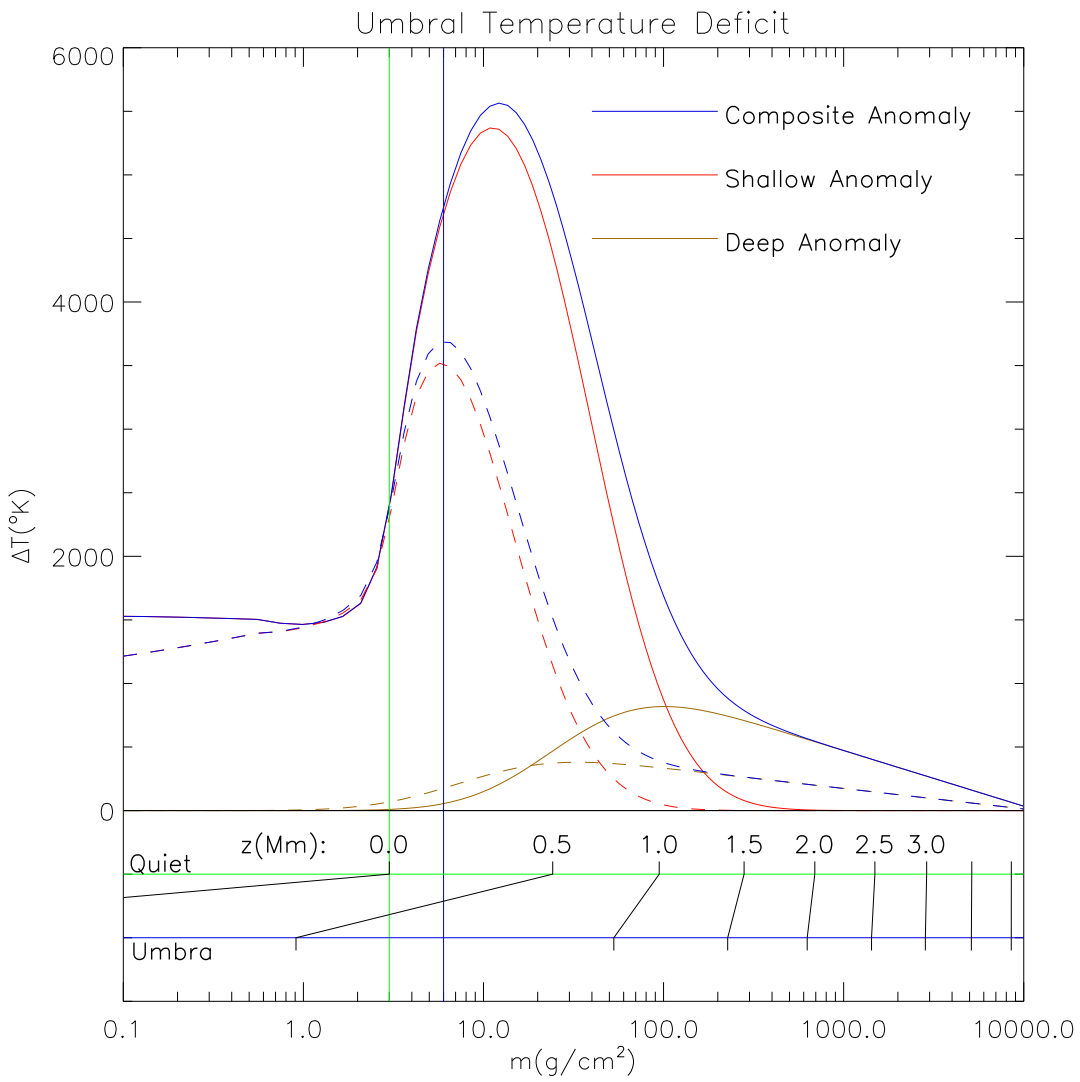

Figure 5: The thermal anomaly of the LRRMC-25 umbra is represented by solid curves in terms of its temperature deficit, ΔT, with respect to that of the quiet Sun at the same column mass density, m. Dashed curves represent the same for an empirical model, GHSE-07, fashioned to satisfy the observations summarized in Figures 2 and 3.

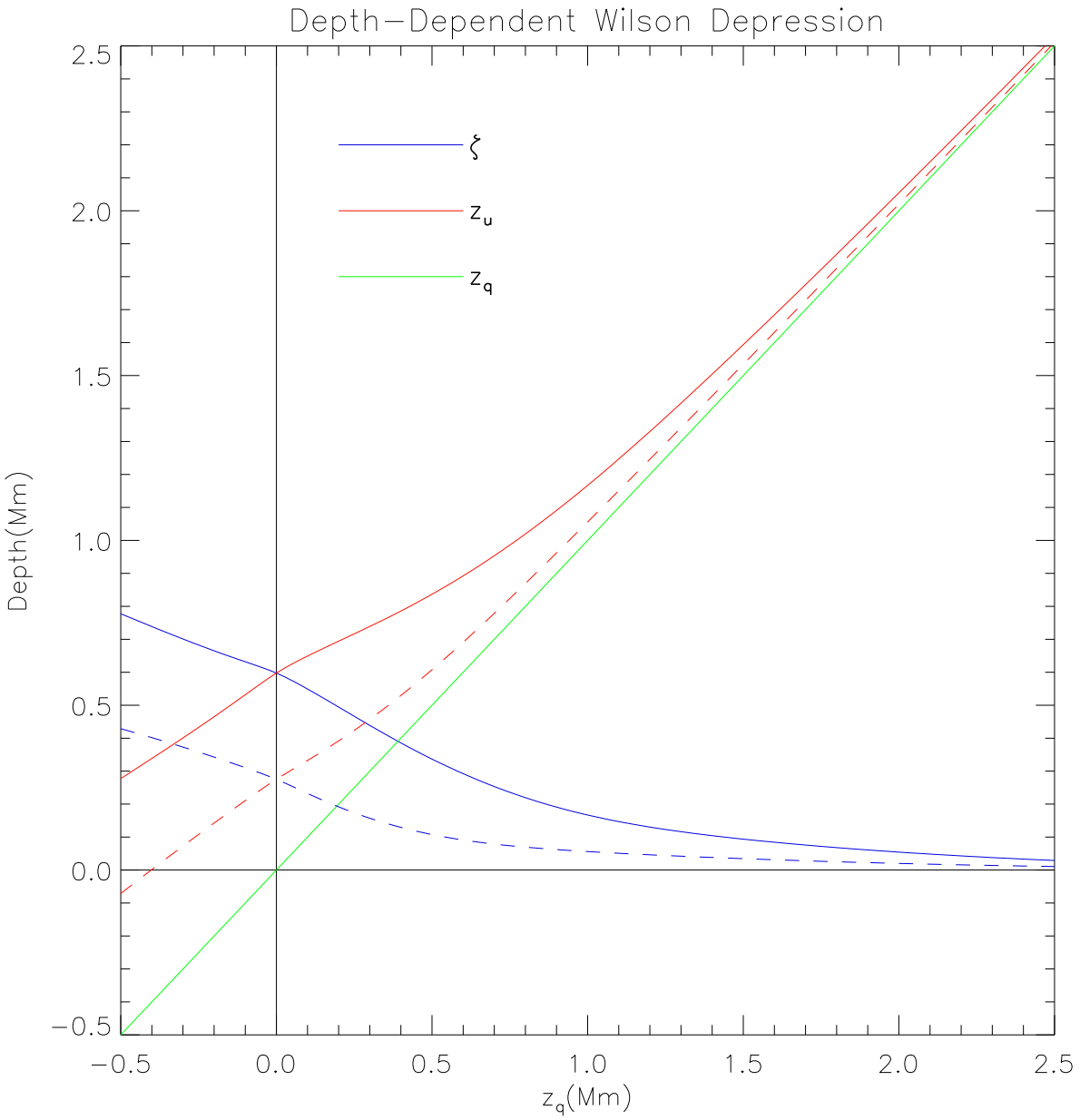

Figure 6: Umbral models LRRMC-25 (solid curves) and GHSE-07 (dashed) represented in terms of depth-dependent Wilson depressions.

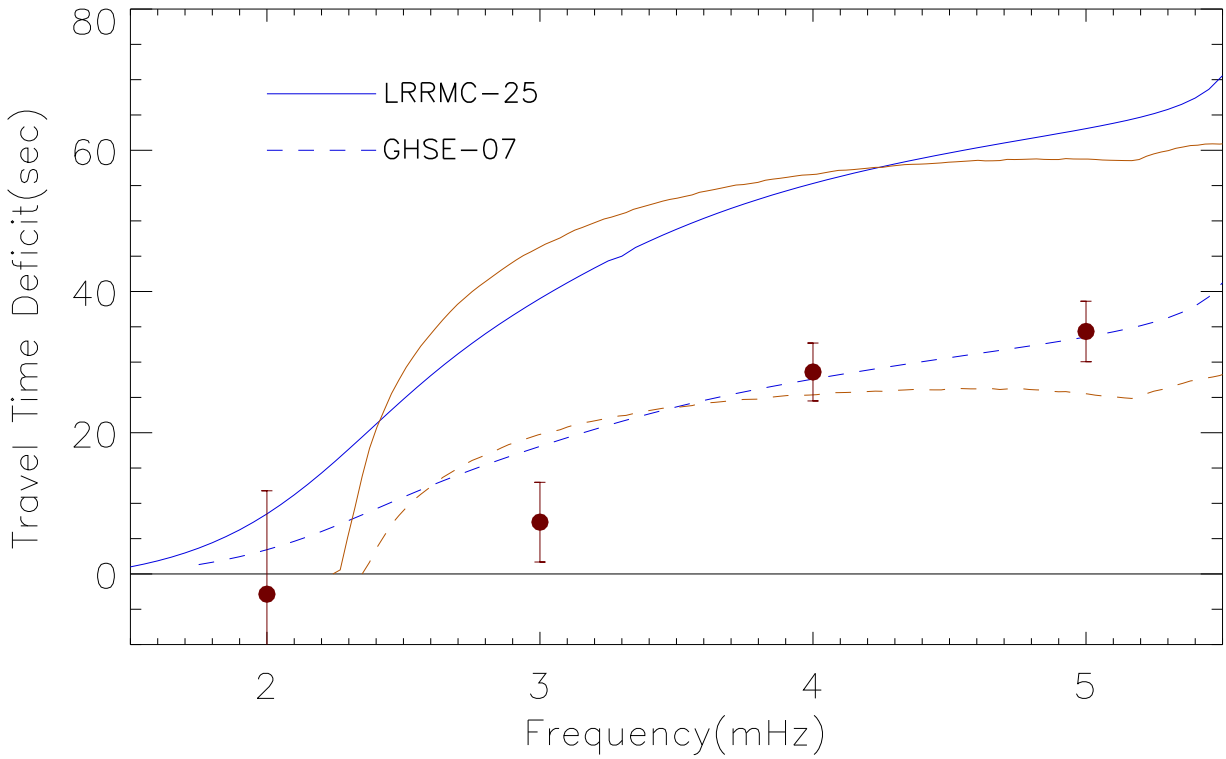

Figure 7: Helioseismic travel times for Umbral models LRRMC-25 (solid curves) and GHSE-07 (dashed) compared with helioseismic travel-time measurements.

How Do We Account Express Non-Adiabatic Acoustics?

Linear Wave Mechanics in a Gravitationally Stratified Medium

We propose to express linear wave mechanics with an account for local heat losses by the following:

$$\frac{\partial^2 \boldsymbol{\xi}}{\partial t^2} \;=\; \frac{1}{\rho_0}\nabla \delta p \;-\; \mathbf{g}\nabla\cdot\boldsymbol{\xi} \;+\; \nabla(\mathbf{g}\cdot\boldsymbol{\xi}), \qquad (1.1)$$

where δp represents the local pressure variation in the medium due to an acoustic disturbance, and this is influenced both by compression and heating or cooling. In familiar adiabatic acoustics,

$$\delta p \;=\; \kappa_S \nabla\cdot\boldsymbol{\xi}, \qquad (1.2)$$

where κ_S is the adiabatic modulus,

$$\begin{aligned} \kappa_S \;&\equiv\; V\Big(\frac{\partial p}{\partial V}\Big)_S \\ &=\; \gamma V\Big(\frac{\partial p}{\partial V}\Big)_T, \end{aligned} \qquad (1.3)$$

and

$$\gamma \;\equiv\; \frac{C_p}{C_V} \qquad (1.4)$$

is the familiar ratio between the heat capacities at constant pressure and constant volume.

To extend the foregoing formalism to non-adiabatic acoustics, we introduce the temperature perturbation, δT, of the disturbance and recognize the pressure variation as a sum of two components:

$$\delta p \;\equiv\; \kappa_T \nabla \cdot \boldsymbol{\xi} \;+\; \beta_V \delta T, \tag{1.5}$$

where

$$\kappa_T \;\equiv\; V\Big(\frac{\partial p}{\partial V}\Big)_T \tag{1.6}$$

is the isothermal modulus and

$$\beta_V \;\equiv\; \Big(\frac{\partial p}{\partial T}\Big)_V. \tag{1.7}$$

We note that

$$\kappa_S \;\equiv\; \gamma \kappa_T. \tag{1.8}$$

Equation (1.1) now becomes

$$\frac{\partial^2 \boldsymbol{\xi}}{\partial t^2} \;=\; \frac{1}{\rho_0}\nabla(\kappa_T \nabla\cdot\boldsymbol{\xi} \;+\; \beta_V \delta T) \;-\; \mathbf{g}\nabla\cdot\boldsymbol{\xi} \;+\; \nabla(\mathbf{g}\cdot\boldsymbol{\xi}). \tag{1.9}$$

Having introduced the temperature perturbation, δT, we need to prescribe how it responds to an acoustic disturbance. We express this by

$$\frac{\partial \delta T}{\partial t} \;=\; \alpha_S \nabla \cdot \frac{\partial \boldsymbol{\xi}}{\partial t} \;-\; \frac{1}{C_V}\frac{\partial Q}{\partial t}, \tag{1.10}$$

where

$$\alpha_S \;\equiv\; V\Big(\frac{\partial T}{\partial V}\Big)_S \;=\; -\frac{VT}{C_V}\Big(\frac{\partial P}{\partial T}\Big)_V, \tag{1.11}$$

and the term $\partial Q/\partial t$ expresses local heat losses by conduction or radiation.

For horizontally invariant mechanics, $\boldsymbol{\xi} \to \xi$, $\nabla \to \partial/\partial z$, and the two terms on the right of equation (1.1) (bouyancy and slosh) cancel. Equations (1.9) and (1.10) therefore become

$$\frac{\partial^2 \xi}{\partial t^2} \;=\; \frac{1}{\rho_0}\Big(\frac{\partial}{\partial z}\kappa_T \frac{\partial \xi}{\partial z} \;+\; \beta_V \delta T\Big), \tag{1.12}$$

and

$$\frac{\partial \delta T}{\partial t} \;=\; \alpha_S \frac{\partial^2 \xi}{\partial z \partial t} \;-\; \frac{1}{C_V}\frac{\partial Q}{\partial t}, \tag{1.13}$$

respectively.

The Radiative-Transfer Problem

The Atmospheres

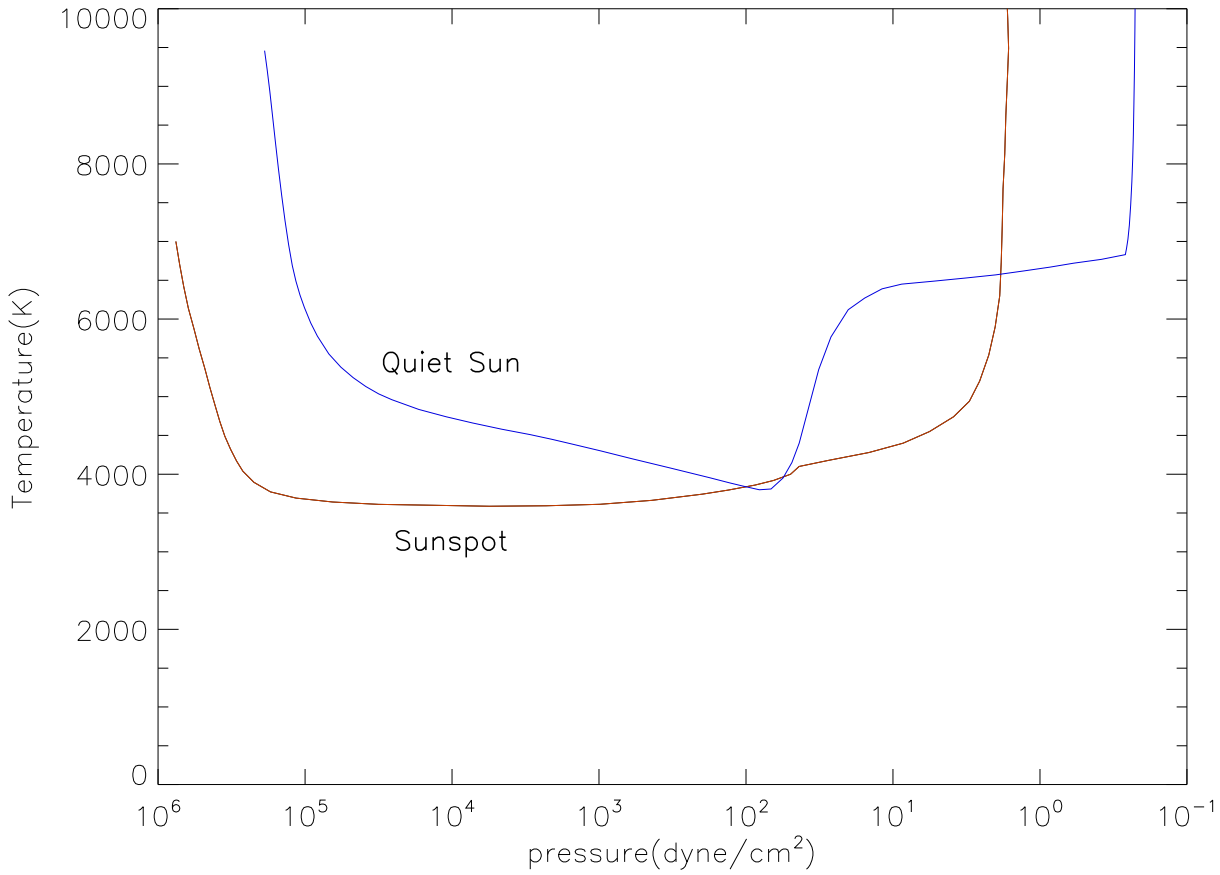

Figure 8: Temperature profiles of the outer atmospheres of the quiet Sun (Fontenla, Averett & Loeser 2002) and a sunspot umbra (Maltby et al. 1986).

Thermal Perturbation

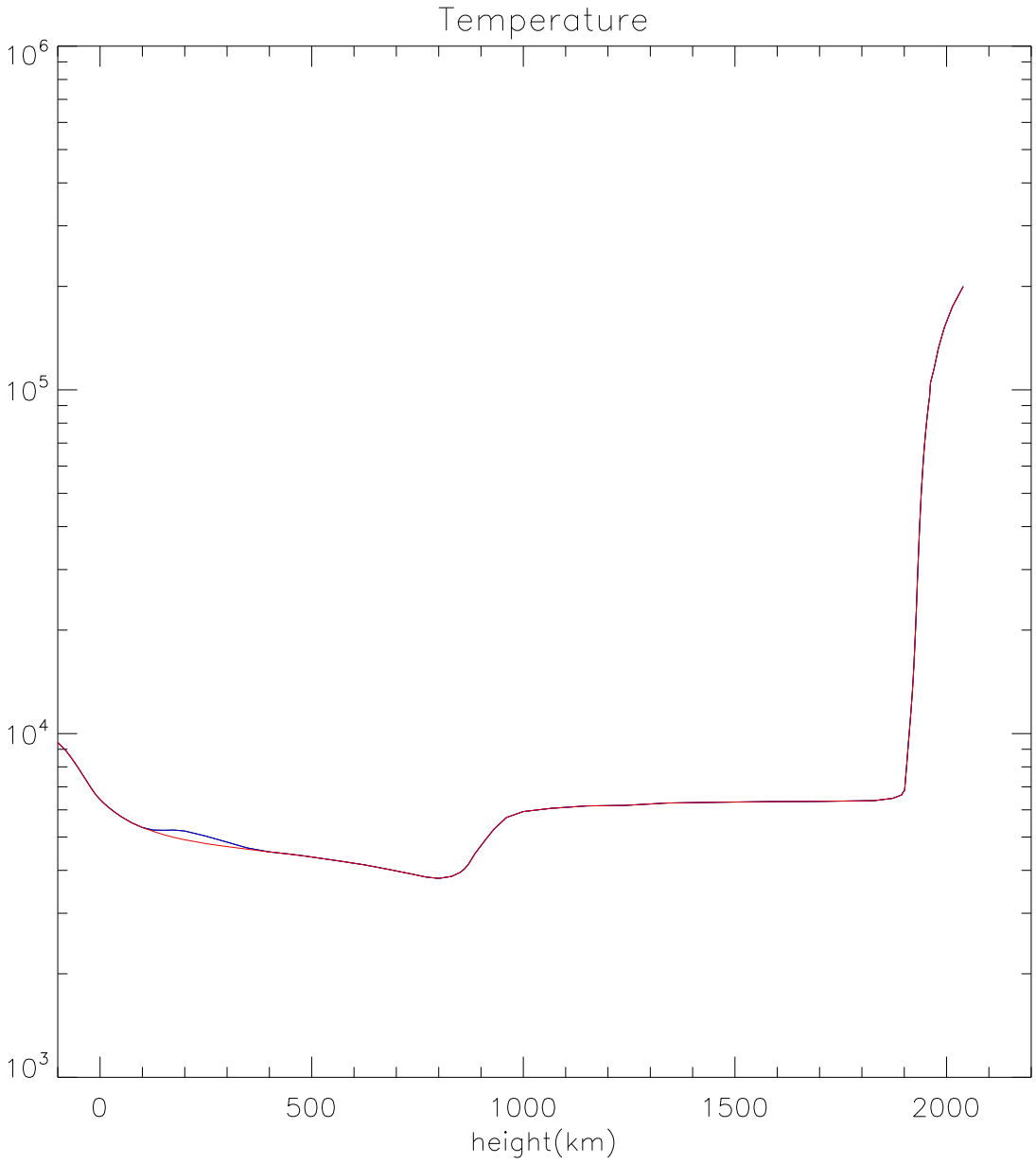

Figure 9: Temperature perturbation introduced into the quiet-Sun model of Fontenla, Averett & Loeser 2002.

Density Perturbation (null in this instance)

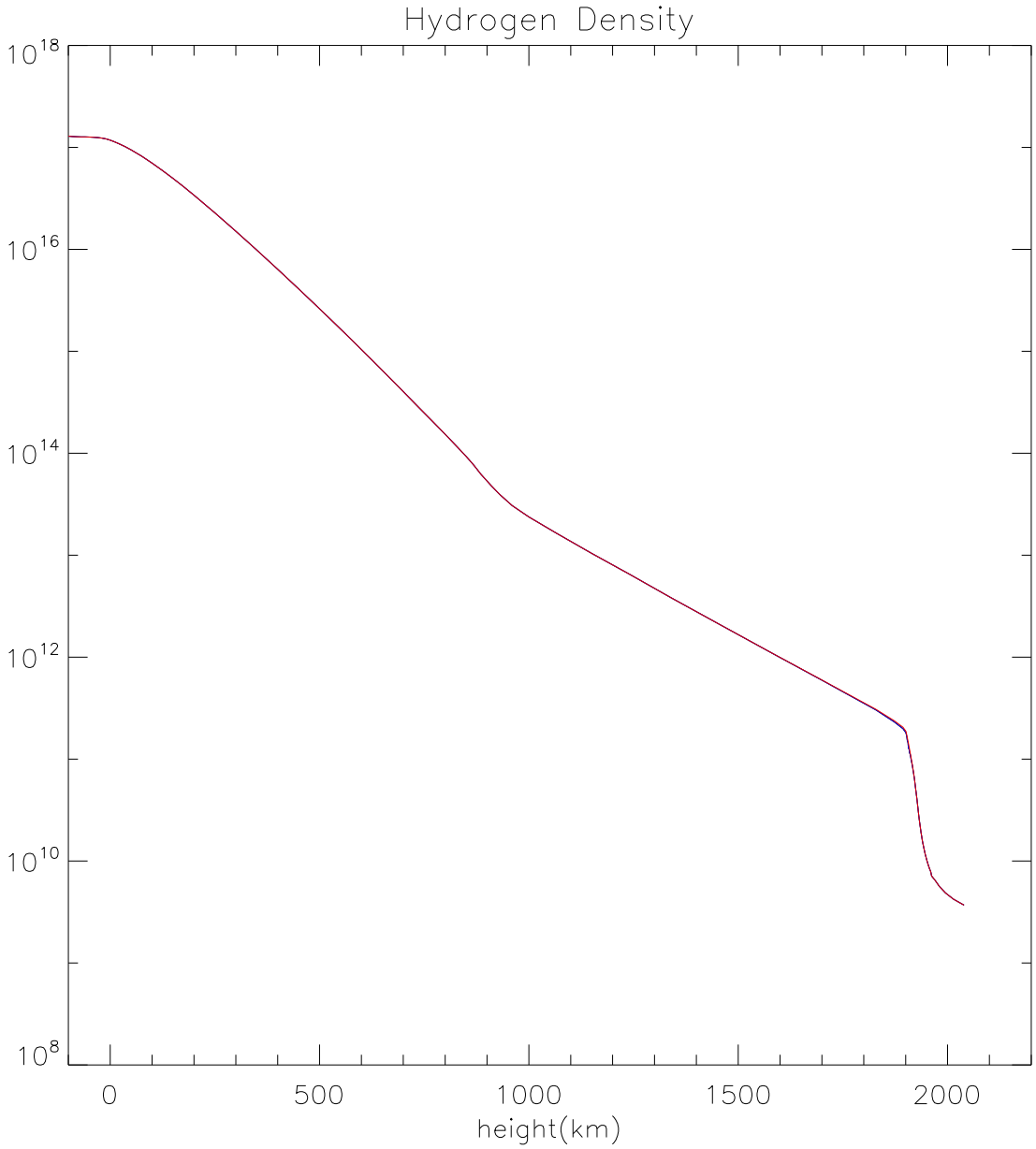

Figure 10: Hydrogen-density profile of the quiet-Sun model of Fontenla, Averett & Loeser 2002.

Temperature Perturbation (photosphere)

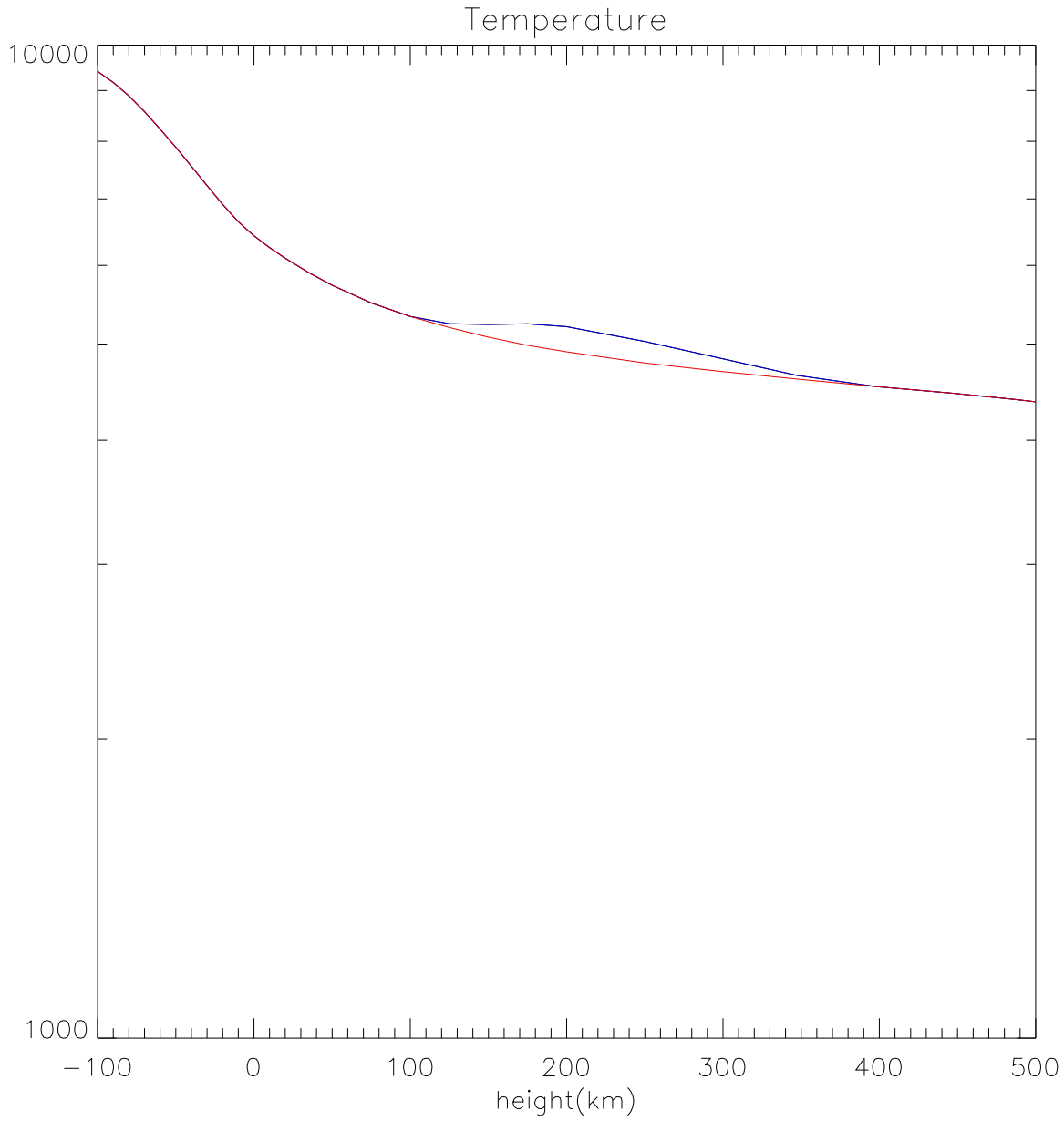

Figure 11: Photospheric temperature perturbation introduced into the quiet-Sun model of Fontenla, Averett & Loeser 2002.

Radiative-Loss Computations

Juan Fontenla uses a 24-node grid engine at NWRA to run the solve the non-LTE RT equations for the unperturbed and perturbed atmospheres, the perturbations being both in temperature and density, the latter preserving column mass density. Radiative losses are compiled in the following spectral intervals:

Designation	Spectral Range
Near UV	100–300 nm
Blue Light	300–500 nm
Red Light	500–1000 nm
Near IR	1–3 μm
Farish IR	3–10 μm

Radiative Losses (Near UV)

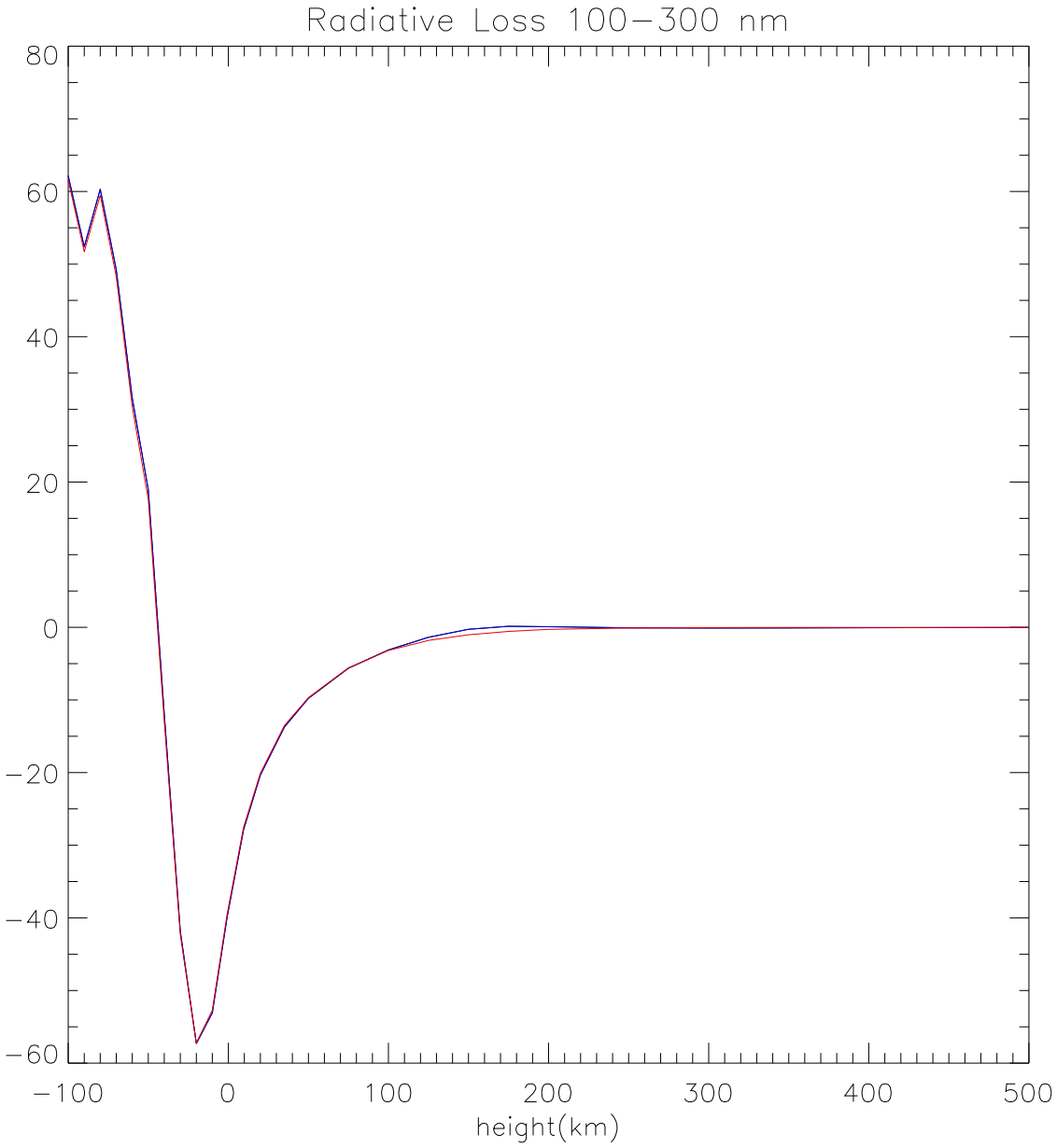

Figure 12: Radiative-loss profile for the thermal perturbation introduced in Figure 11 in the near UV spectrum.

Radiative Losses (Blue Light)

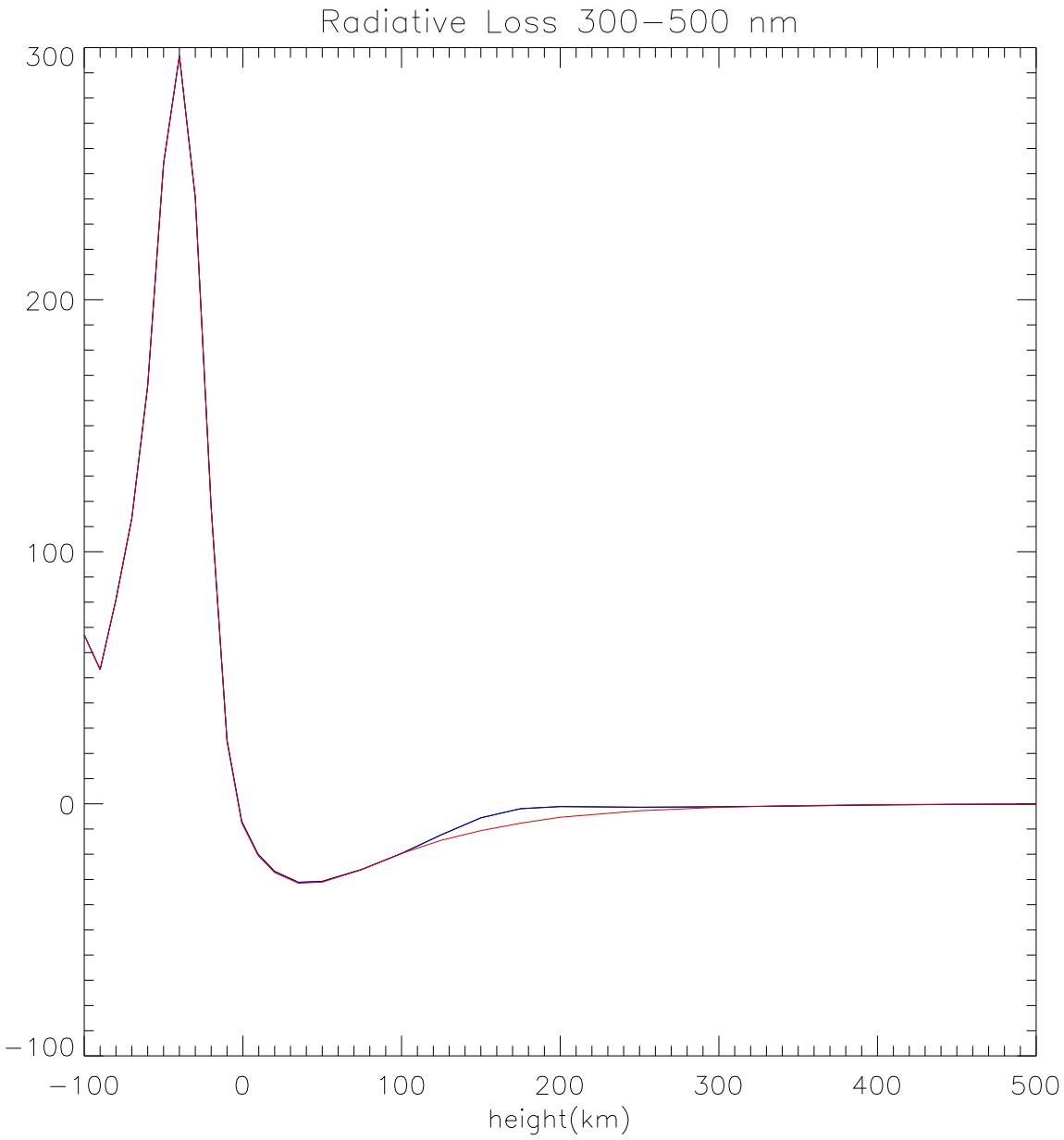

Figure 13: Radiative-loss profile for the thermal perturbation introduced in Figure 11 in blue light.

Radiative Losses (Red Light)

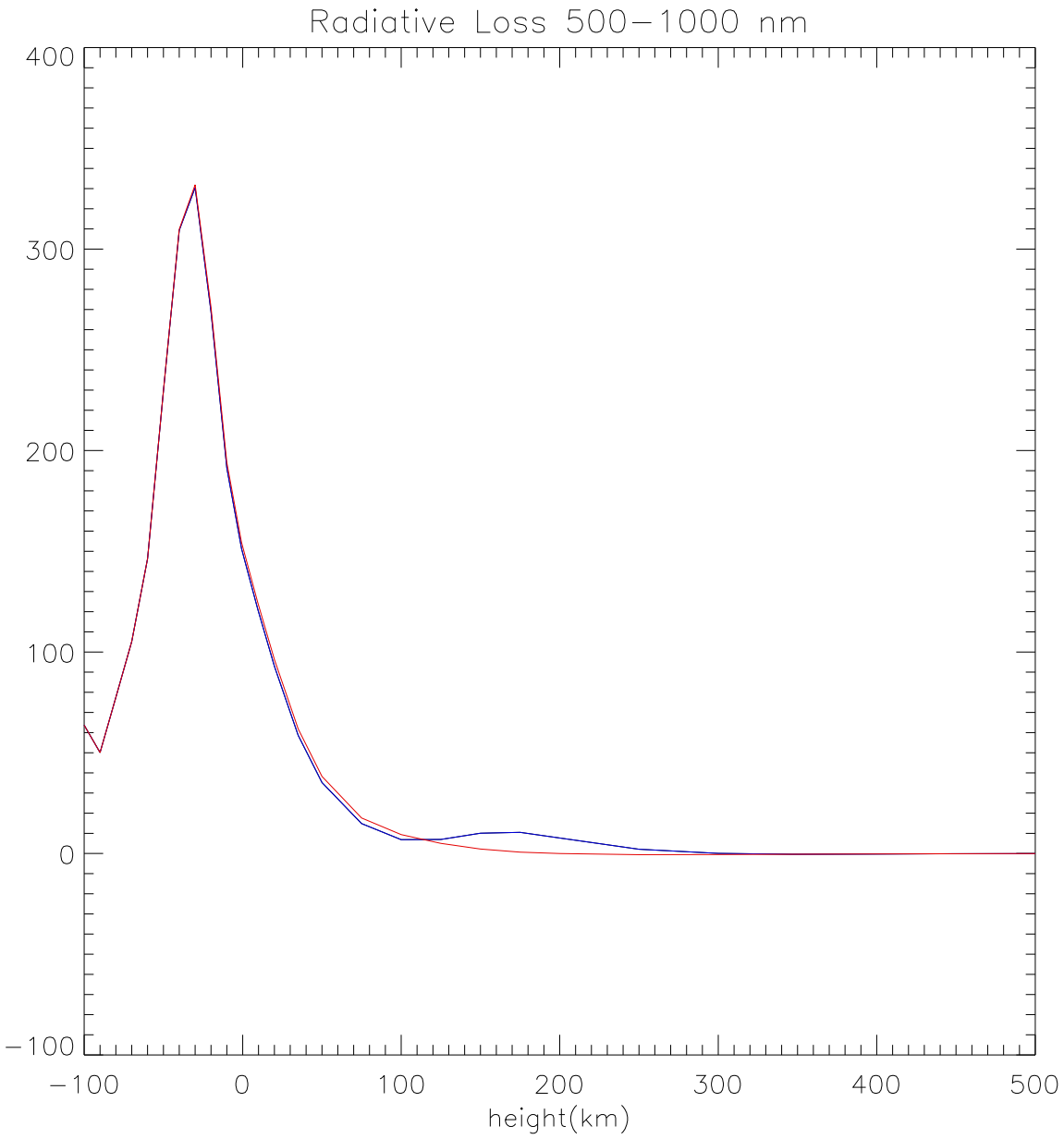

Figure 14: Radiative-loss profile for the thermal perturbation introduced in Figure 11 in red light.

Radiative Losses (Near IR)

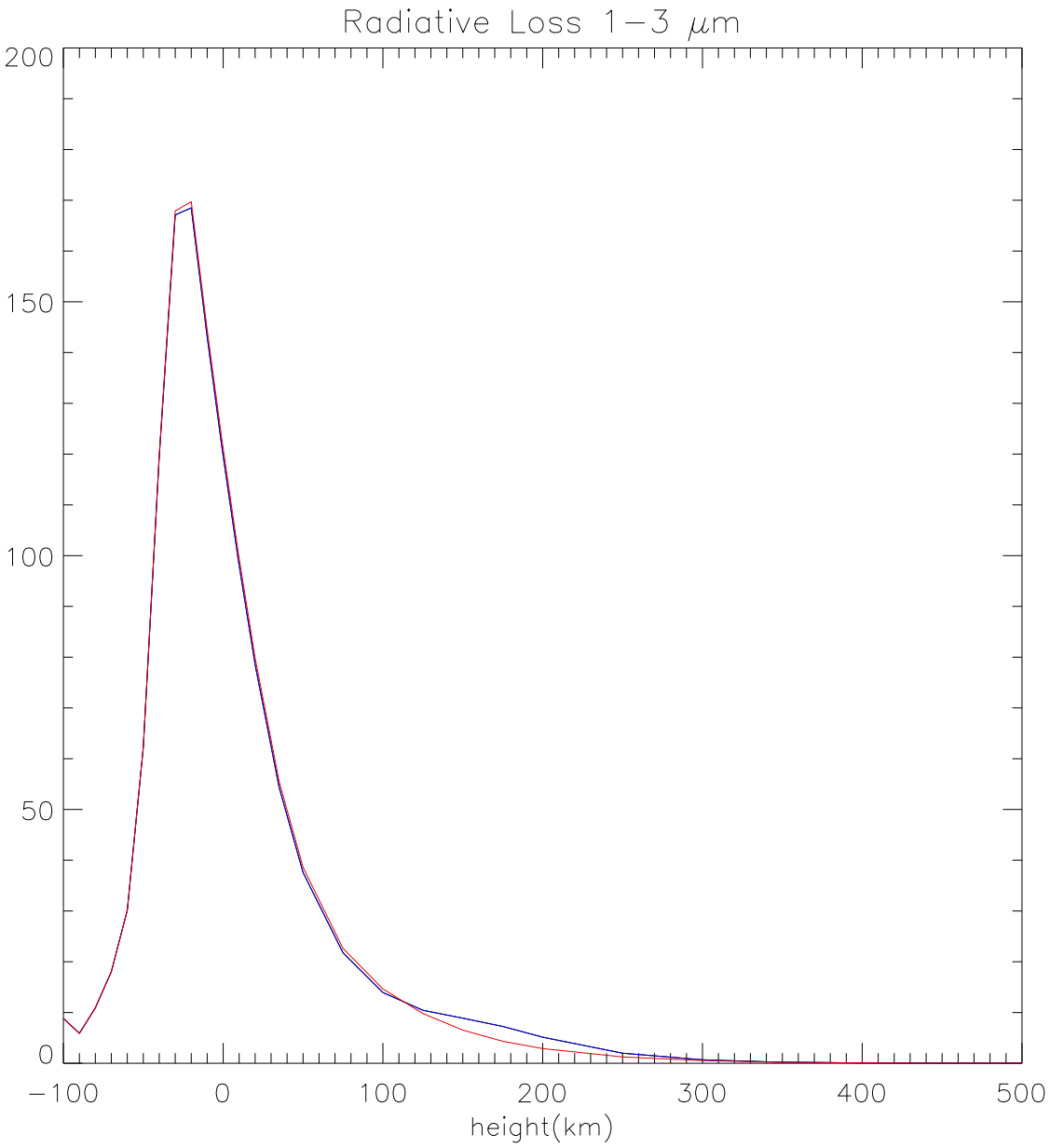

Figure 15: Radiative-loss profile for the thermal perturbation introduced in Figure 11 in the near IR spectrum.

Radiative Losses (Farish IR)

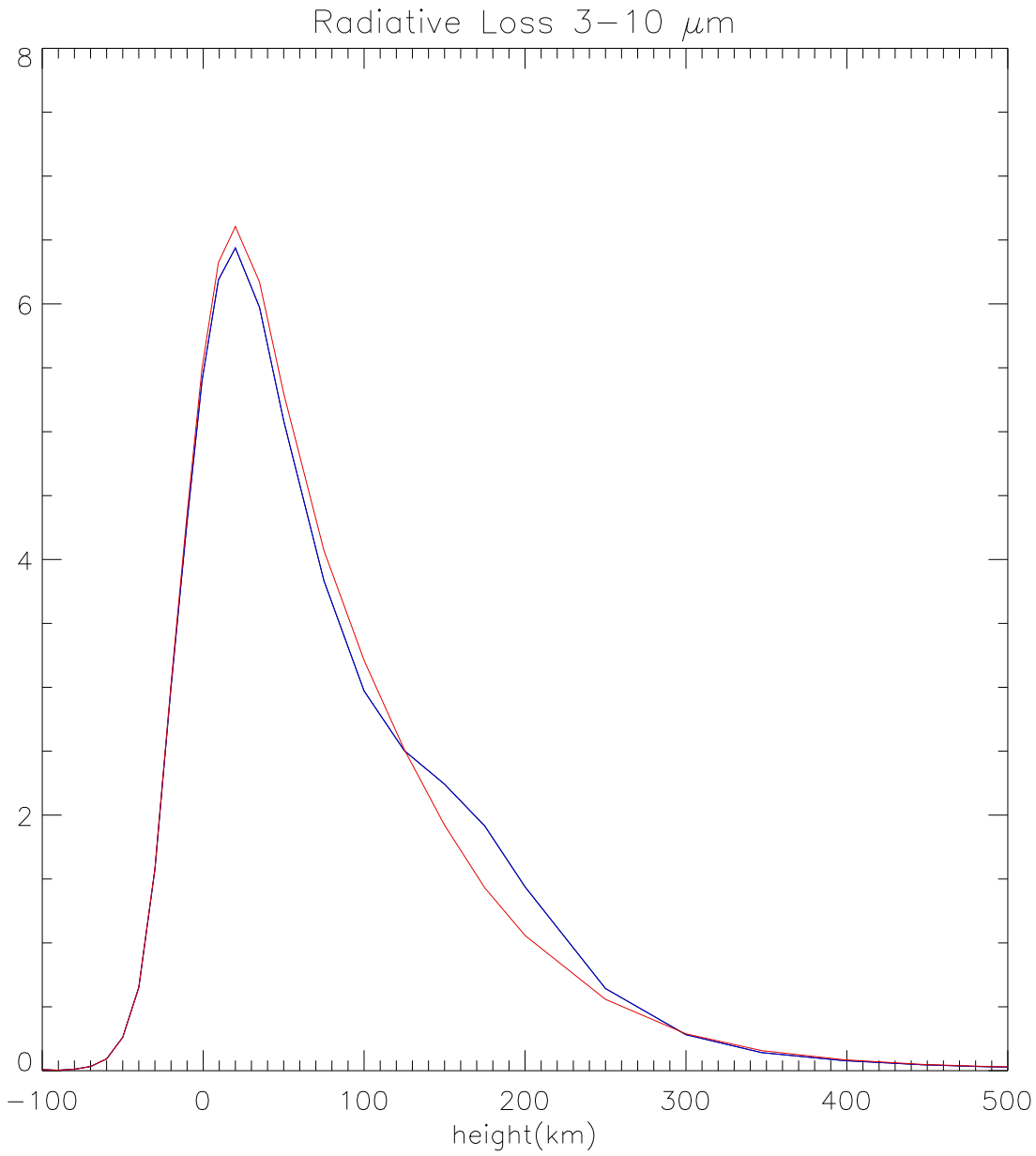

Figure 16: Radiative-loss profile for the thermal perturbation introduced in Figure 11 in the not-so-near IR spectrum.

Putting Acoustics and RT Together

Primary task: Due to considerations of precision, the RT computations are conducted with perturbations that are relatively broad in depth (∼100 km) compared to what we need in acoustic resolution (∼10 km). This introduces the (forward modeling) problem of devising kernels, $Q_t(z, z_0)$, that, when smeared by the distributions, $K(z, z', z_0)$, prescribed by Juan Fontenla's perturbation profiles, lead to the radiative-loss perturbations, $Q_t^{\rm JF}$, consistent with Juan Fontenla's computations:

$$Q_t^{\rm JF}(z,\ z_0)\ =\ \int_{-\infty}^{\infty} K(z,\ z',\ z_0)\ Q_t(z',\ z_0)\ dz', \tag{2.1}$$

where

$$Q_t(z,\ z_0)\ =\ \epsilon\delta(z\ -\ z_0)\ +\ {\rm an}(\tau_{\rm gray}). \tag{2.2}$$

This appears to be fairly straight-forward under certain simplifying assumptions. NWRA postdoc Cris Clack is working on a formalism to express these kernels in terms of analytic functions with parameters that vary smoothly with depth, assuming LTE RT in a piece-wise gray medium.

Summary

- An account of non-adiabatic acoustics, in both active regions and the quiet Sun is essential for a reliable understanding of seismic signatures in active-region photospheres.
- The major component of non-adiabatic mechanics in photospheric acoustics is that introduced by radiative exchange of heat in the photosphere and chromosphere and the thermal relaxation that results therefrom.
- An credible account for the effects of radiative transfer in photospheric helioseismic signatures appears to be possible. One-dimensional simulations of photospheric and chromospheric acoustics offers intuitive insight into this question that is likely to be valuable.